

Article

Effect of Preparation Methods on the Performance of Pt/TiO₂ Catalysts for the Catalytic Oxidation of Carbon Monoxide in Simulated Sintering Flue Gas

Jianyu Cai, Zehui Yu and Jian Li *

Key Laboratory of Beijing on Regional Air Pollution Control, Beijing University of Technology, Beijing 100124, China; caijy@emails.bjut.edu.cn (J.C.); yuzehui@emails.bjut.edu.cn (Z.Y.)

* Correspondence: ljian@bjut.edu.cn; Tel.: +86-10-6739-2080

Abstract: A series of Pt/TiO₂ catalysts were prepared by the impregnation (IM), dry ball mill (DB), or wet ball mill (WB) methods, and their catalytic activity for the oxidation of CO was evaluated. The structure and redox properties of the catalysts were investigated by N₂ desorption, XRD, SEM, TEM, XPS, H₂-TPR, SO₂-TPD, and CO chemisorption analysis. It was determined that the preparation method affects the physical structure of the catalyst and the particle size and dispersion of Pt on the catalyst surface. The catalyst prepared by the impregnation method had a more suitable physical structure than the other catalysts, with a smaller particle size, a higher dispersion of Pt on the surface, and the lowest strength of SO₂ adsorption. Pt/TiO₂(IM) catalysts presented the best catalytic activity for the oxidation of CO in simulated sintering flue gas at 140 °C, as well as better sulfur and water resistance with simulated sintering flue gas containing 50 ppm of SO₂ and 15% water vapor.

Keywords: CO oxidation; preparation method; influence on performances; sulfur and water resistance



Citation: Cai, J.; Yu, Z.; Li, J. Effect of Preparation Methods on the Performance of Pt/TiO₂ Catalysts for the Catalytic Oxidation of Carbon Monoxide in Simulated Sintering Flue Gas. *Catalysts* **2021**, *11*, 804. <https://doi.org/10.3390/catal11070804>

Academic Editors: Manas Sutradhar and Tannistha Roy Barman

Received: 7 June 2021

Accepted: 30 June 2021

Published: 30 June 2021

Publisher's Note: MDPI stays neutral with regard to jurisdictional claims in published maps and institutional affiliations.



Copyright: © 2021 by the authors. Licensee MDPI, Basel, Switzerland. This article is an open access article distributed under the terms and conditions of the Creative Commons Attribution (CC BY) license (<https://creativecommons.org/licenses/by/4.0/>).

1. Introduction

Carbon monoxide (CO) is both a major air pollutant and a potentially valuable resource. CO is produced by a wide range of sources, including industrial production [1] and fuel combustion [2,3]. However, due to its flammability, explosive limits, and toxicity, CO emissions often cause poisoning and accidental fires [4]. Due to the risks of CO emissions, many countries around the world are increasing the regulation of CO. CO management methods include catalytic oxidation [5,6], adsorption [7], cryogenic separation [8], and co-adsorption [9].

Catalytic oxidation is one of the most effective methods for the removal of CO [10], and supported Pt catalysts are commonly reported to show good catalytic activity for CO oxidation [11]. Presently, research on supported Pt and other precious metal catalysts is focused on improving the low-temperature catalytic activity by adjusting the particle size of the precious metal particles [12], improving the dispersion of the precious metals on the catalyst support [13], using additives to change the electronic state of the precious metals [14], and adjusting the local structure effect of active sites [15].

The preparation method is an important factor affecting the performance of catalysts. The key to improving the catalytic performance of supported catalysts is adjusting the size and morphology of the catalysts [16], which are significantly affected by the choice of preparation method. Ince et al. [17] reported that the shape of Pt metal catalysts affected their performance in CO catalytic oxidation. Son et al. [18] found that Pt catalysts synthesized by different preparation methods had different structural characteristics, such as spherical, pyramid, dumbbell, or cube morphologies. Boubnov et al. [19] reported that different preparation methods affected the pore structure inside and between catalyst particles, affecting both the dispersion of Pt on the surface of the catalyst and the performance of the catalyst. The preparation method can also affect the dispersion of noble metal particles in

supported catalysts [20]. The good dispersion of precious metals on the catalyst support is critical for achieving high catalytic activity [21,22]. Many Pt catalysts with a high level of dispersion and small particle sizes have been reported to show enhanced CO oxidation activity [23]. The chemical state of Pt species also affects catalytic activity. Hong and Sun [24] compared the CO oxidation catalytic activity of Pt/CeO₂ catalysts prepared by impregnation, deposition–precipitation, and impregnation–reduction methods, ultimately finding that the preparation method affected the presence of Pt species. Their catalyst prepared by impregnation–reduction had more negatively charged metallic Pt species and showed the best catalytic activity compared with catalysts prepared by impregnation or deposition–precipitation.

In this study, a series of Pt/TiO₂ catalysts were prepared by impregnation, dry ball milling, and wet ball milling methods for the first time. The CO oxidation catalytic activity of the Pt/TiO₂ catalysts was compared and the effects of different preparation methods on the structure and performance of the catalysts were explored through a series of characterization methods. The preparation methods selected in this study are all simple and convenient. Through comparative study, the most suitable preparation methods for industrial production are selected.

2. Results and Discussion

2.1. Catalytic Performance

Figure 1 shows the activities of Pt/TiO₂ catalysts with different preparation methods for the oxidation of CO. All three catalysts did not show catalytic activity at 60 °C, but their activity increased with temperature. [24]. For the Pt/TiO₂(IM) and Pt/TiO₂(DB) catalysts, a 100% CO removal efficiency was achieved at 140 °C (the test conditions ensured that the inlet CO concentration was about 8000 ppm). When the CO removal efficiency reached 100%, the MRU infrared flue gas analyzer showed that the amount of CO left in the products stream was 0 ppm. However, the precision and the resolution of the instrument were 1% and 1 ppm, respectively, so the CO amount left in the products stream did not exceed 80 ppm. However, for the Pt/TiO₂(WB) catalysts, the CO removal efficiency at 140 °C was only 30%, and the 100% removal of CO was not achieved until 160 °C. Below 130 °C, the catalytic activity of Pt/TiO₂(IM) was significantly higher than that of Pt/TiO₂(DB) and Pt/TiO₂(WB). These results showed that Pt/TiO₂(IM) catalysts have the highest catalytic activity for CO oxidation, followed by Pt/TiO₂(DB) and then Pt/TiO₂(WB), which showed the lowest activity over the examined temperature range.

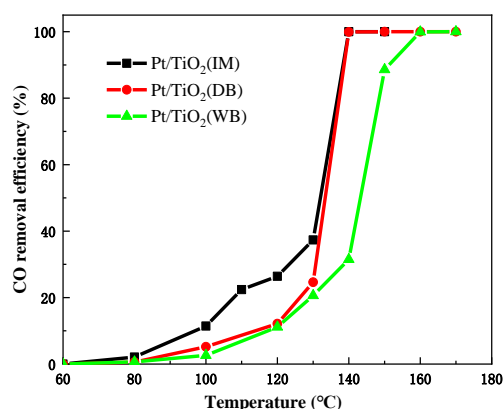


Figure 1. Activity of Pt/TiO₂ catalysts for the catalytic oxidation of CO. Pt/TiO₂(IM), Pt/TiO₂(DB), and Pt/TiO₂(WB) represent the catalysts prepared by impregnation, dry ball mill, and wet ball mill, respectively.

The results of the stability tests of the catalysts at 170 °C in the presence of SO₂ and water vapor are shown in Figure 2. After 12 h of continuous testing, differing behavior was seen in the catalysts prepared by different methods. The catalyst performance of

Pt/TiO₂(IM) did not change, maintaining the 100% removal of CO after 12 h. The catalyst performance of Pt/TiO₂(WB) decreased slightly from 100% to 99.7%. However, the catalyst performance of Pt/TiO₂(DB) significantly decreased and also fluctuated, with the removal rate of CO decreasing to 99%. There were four possible reasons for the poisoning of catalyst A: the first possible cause was the sintering of Pt particles, the second possible cause was the coverage of Pt particles by SO_x species, the third possible cause was the formation of Pt sulfate species, and the fourth possible cause was the formation of TiOSO₄, which affected the interfacial action. Smirnov [25] found that SO₂ was oxidized to SO₃ at the Pt sites and then quickly migrated to the carriers. In addition, Taira and Einaga [26] explored the influence mechanism of H₂O and SO₂ on the Pt/TiO₂ catalyst, finding that in the presence of both SO₂ and H₂O, the generation of TiOSO₄ covered the catalyst surface, resulting in deactivation. Combined with previous studies, the first three conjectures of catalyst poisoning could be eliminated. It could be speculated that in the presence of SO₂ and water vapor in these stability tests, the three catalysts were poisoned due to the generation of TiOSO₄, resulting in the decline of catalytic performance.

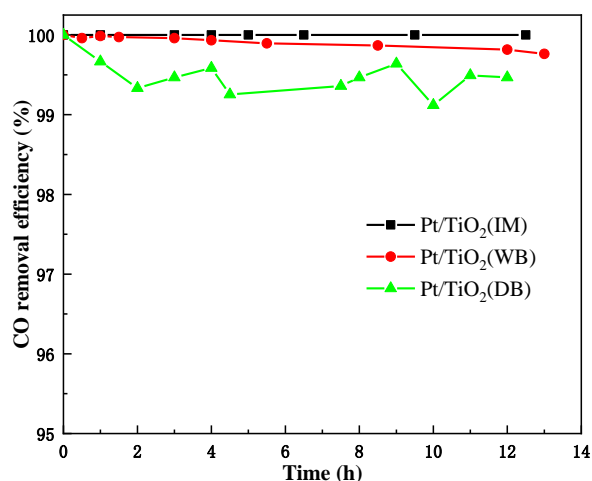


Figure 2. Activity of Pt/TiO₂ catalysts for the catalytic oxidation of CO in the presence of SO₂ and water vapor.

2.2. Catalyst Characterization

2.2.1. BET

A number of analyses were performed to identify the effect of the different preparation methods on the Pt/TiO₂ catalysts. Physical property data of TiO₂ and Pt/TiO₂ catalysts are provided in Table 1. Pt/TiO₂(IM)-SH, Pt/TiO₂(DB)-SH, and Pt/TiO₂(WB)-SH represent the catalyst after SO₂ poisoning, while Pt/TiO₂(IM), Pt/TiO₂(DB), and Pt/TiO₂(WB) represent fresh catalysts. The BET surface area, pore volume, and pore size of the fresh catalysts differed based on the preparation method. These differences were potentially because when Pt particles are loaded on TiO₂, they cover some of the specific surface area and enter and block the pores in TiO₂ [27]. It is worth noting that the pore volume and pore size of both the Pt/TiO₂(DB) and Pt/TiO₂(WB) catalysts were significantly reduced compared with the pore volume and pore size of Pt/TiO₂(IM). It can be inferred that the mechanical force of ball milling caused the catalyst pores to collapse and particles to agglomerate. The BET surface area, pore volume, and pore size of Pt/TiO₂(WB) were larger than those of Pt/TiO₂(DB), which was potentially because the solvent added in Pt/TiO₂(WB) acted as a buffer to reduce the effect of mechanical forces during the ball milling process. Overall, the values of BET surface area, pore volume, and pore size for the fresh catalysts followed the trend of Pt/TiO₂(IM) > Pt/TiO₂(WB) > Pt/TiO₂(DB). These results showed that different preparation methods had a significant influence on the physical properties of Pt/TiO₂ catalysts.

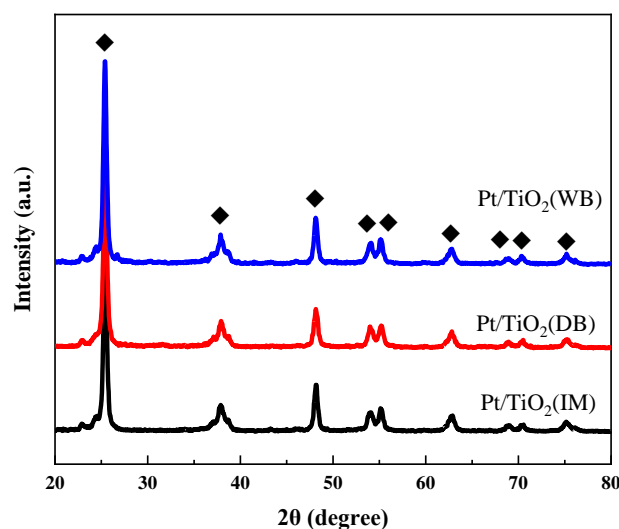
Table 1. Physical property data of TiO₂ and Pt/TiO₂ catalysts.

Catalyst	BET Surface Area m ² ·g ⁻¹	Pore Volume cm ³ ·g ⁻¹	Pore Size nm
TiO ₂	83	0.513	27.2
Pt/TiO ₂ (IM)	79	0.411	20.7
Pt/TiO ₂ (DB)	64	0.182	11.4
Pt/TiO ₂ (WB)	78	0.330	16.7
Pt/TiO ₂ (IM)-SH	67	0.290	17.4
Pt/TiO ₂ (DB)-SH	55	0.156	11.2
€Pt/TiO ₂ (WB)-SH	66	0.272	16.3

The BET surface area, pore volume, and pore size of the catalysts after SO₂ poisoning showed a similar trend. Combined with the catalyst test results in Figure 2, the decay rate of CO oxidation catalytic performance in the presence of SO₂ and water vapor was as follows: Pt/TiO₂(DB) > Pt/TiO₂(WB) > Pt/TiO₂(IM). This was consistent with the trend in the BET surface area, pore volume, and pore size of the three catalysts. Combined with the results of Taira and Einaga [26], it can be inferred that TiOSO₄ was generated on the catalyst surface in the presence of SO₂ and water vapor, resulting in a decrease in BET surface area, pore volume, and pore size, which accelerated the degradation of catalyst performance. That is to say, the Pt/TiO₂(DB) catalyst, with the lowest BET surface area, pore volume, and pore size, also had the lowest stability in the presence of SO₂ and water vapor.

2.2.2. XRD

The influence of the preparation method on the crystal structure of the Pt/TiO₂ catalysts was investigated by XRD. Figure 3 shows the XRD patterns of fresh Pt/TiO₂(IM), Pt/TiO₂(DB), and Pt/TiO₂(WB) catalysts obtained using a 2θ range of 20°–80°. All three catalysts presented typical TiO₂ diffraction peaks at 2θ = 25.3°, 37.8°, 48°, 53.9°, 55°, 62.7°, 68.8°, 70.5°, 75.1°, and 76.1° (JCPDS No.21-1272). The XRD patterns showed that the crystal structure of the TiO₂ support was not affected by different preparation methods. According to the report, the catalysts prepared by anatase TiO₂ had a large specific surface area and a high content of Pt²⁺ phase on the surface. The support could easily form oxygen vacancy and create a super catalytic performance [28]. This was consistent with the results of the catalyst performance test and the valence test of Pt in XPS.

**Figure 3.** XRD patterns of Pt/TiO₂ catalysts.

Diffraction peaks attributed to Pt species were not present, an indication that Pt species were highly dispersed on the TiO₂ support or were below the detection limit [29].

2.2.3. SEM

In order to explore the influence of the preparation method on the structure of the catalysts, scanning electron microscopy was used to observe and compare the difference in surface morphology of the catalysts. Figure 4 shows SEM images of Pt/TiO₂(IM), Pt/TiO₂(DB), Pt/TiO₂(WB), and Pt/TiO₂(IM)-SH. Comparing these images reveals significantly different morphologies. Figure 4a shows small, uniform particles on the surface and a high concentration of uniformly sized pores. Figure 4b shows irregular particles, and due to the severe agglomeration of particles and collapse of the pores, the pores are sparse and significantly irregular. Figure 4c shows a cluster structure with fine, irregular pores, some of which are aggregated into relatively dense clusters. The pore structure is rich, but the pore size is small. It is evident that the preparation method had a strong influence on the structure of Pt/TiO₂ catalysts.

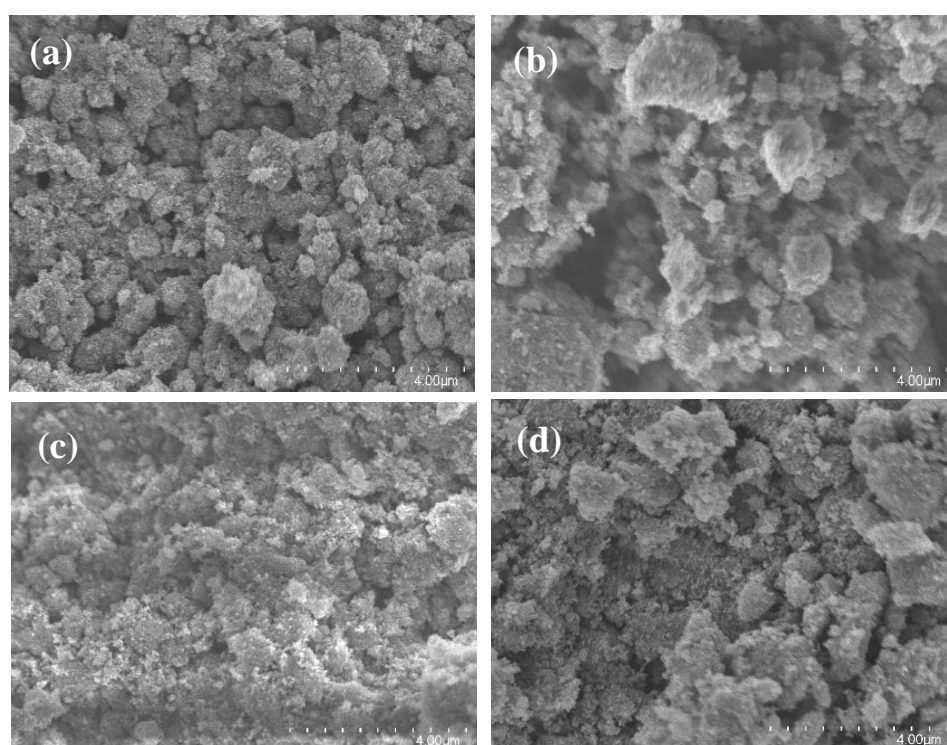


Figure 4. SEM images of (a) Pt/TiO₂(IM), (b) Pt/TiO₂(DB), (c) Pt/TiO₂(WB), and (d) Pt/TiO₂(IM)-SH.

Compared with the fresh catalysts, the SEM image of Pt/TiO₂(IM)-SH shown in Figure 4d shows that significant differences in morphology existed after SO₂ poisoning. Surface particles became larger, the number of pores was lower, and floccus could be seen on the surface of the catalyst. It is speculated that these changes were due to the formation of TiOSO₄ surface of the catalyst.

2.2.4. TEM and CO Chemisorption Test

In order to observe the dispersion of Pt on the surface of TiO₂, TEM and CO chemisorption tests were performed on the three catalysts. TEM images of all three catalysts are shown in Figure 5. Lattices with a spacing of 0.22 nm can be observed in Figure 5a–c, consistent with the lattice spacing of the Pt (111) plane. This demonstrated that Pt was successfully loaded onto the TiO₂ support. Lower-magnification TEM images in Figure 5d–f show that the distribution of Pt on Pt/TiO₂(IM) was relatively uniform. However, Pt species showed significant agglomeration on Pt/TiO₂(DB) and Pt/TiO₂(WB). CO chemisorption tests supported this observation. As can be seen in Table 2, the dispersions of Pt species were 85.06%, 78.25%, and 73.19% on the Pt/TiO₂(IM), Pt/TiO₂(DB), and Pt/TiO₂(WB) catalysts,

respectively. Furthermore, the Pt particle size of Pt/TiO₂(IM) was 8.89 nm, compared with 9.61 and 10.13 nm for Pt/TiO₂(DB) and Pt/TiO₂(WB), respectively. Combined with the catalytic performance test results shown in Figure 1, it can be seen that the CO oxidation catalytic activity of Pt/TiO₂ decreased with an increase in Pt particle size and also with a decrease in Pt dispersion. This was supported by other studies showing that metal particle size and dispersion strongly affected catalytic activity [30–33]. It is evident that the choice of the preparation method affected the CO oxidation catalytic activity of Pt/TiO₂ catalysts by affecting the dispersion and particle size of Pt.

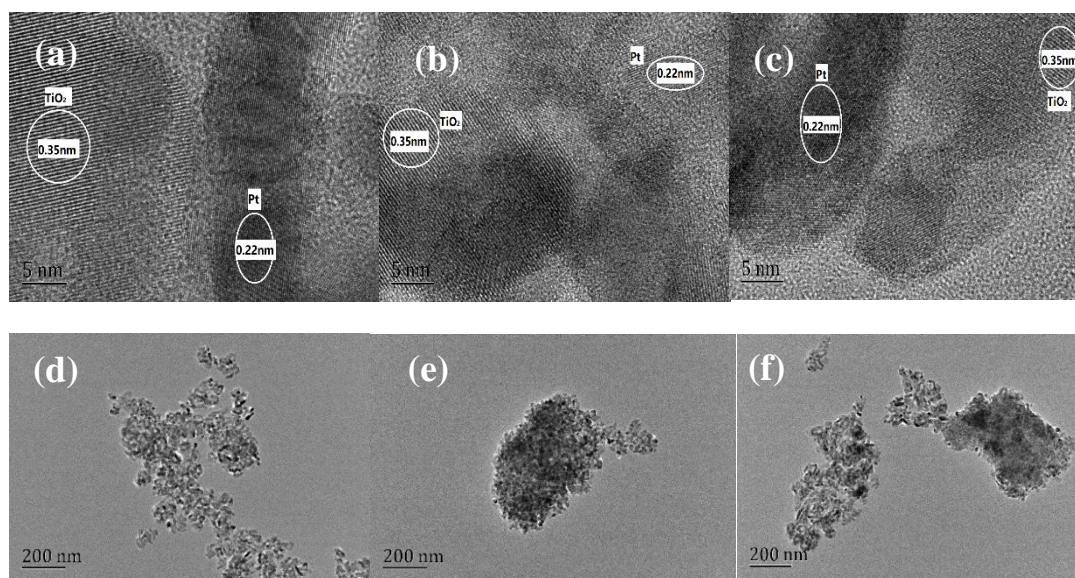


Figure 5. TEM images of (a)/(d) Pt/TiO₂(IM), (b)/(e) Pt/TiO₂(DB), and (c)/(f) Pt/TiO₂(WB).

Table 2. Platinum dispersion, platinum particle size, and platinum surface area of Pt/TiO₂ catalysts determined by CO chemisorption.

Catalyst	Platinum Dispersion %	Platinum Particle Size nm	Platinum Surface Area m ² ·g ⁻¹
Pt/TiO ₂ (IM)	85.06	8.89	0.24
Pt/TiO ₂ (DB)	78.25	9.61	0.09
Pt/TiO ₂ (WB)	73.19	10.13	0.03

2.2.5. H₂-TPR

Figure 6 shows the H₂-TPR profiles of pure TiO₂ and the three Pt/TiO₂ catalysts prepared by different methods. For pure TiO₂, only one reduction peak at 473.3 °C is visible, which is ascribed to the reduction of the superficial lattice oxygen of TiO₂ [34,35]. The H₂-TPR profiles of the Pt/TiO₂ catalysts also show a second reduction peak between 70 and 80 °C, which could be attributed to the reduction process of PtO into metallic Pt [36,37]. Additionally, when Pt was loaded on TiO₂, the reduction peak of the superficial lattice oxygen of TiO₂ moved to lower temperatures, shifting from 473.3 °C to that between 200 and 350 °C. The intensity of the peak, representing the consumption of H₂, also significantly increased for Pt/TiO₂ compared with pure TiO₂. This phenomenon was caused by hydrogen overflow [38], and the results showed that loading Pt on TiO₂ increased the surface oxygen content. Comparing the reduction peaks located between 200 and 350 °C, it can be seen that Pt/TiO₂(IM) had the lowest reduction temperature, followed by Pt/TiO₂(DB) and then Pt/TiO₂(WB). These results are a strong indication that Pt/TiO₂(IM) had the best low-temperature catalytic activity, which is consistent with the results of the catalyst activity tests shown in Figure 1.

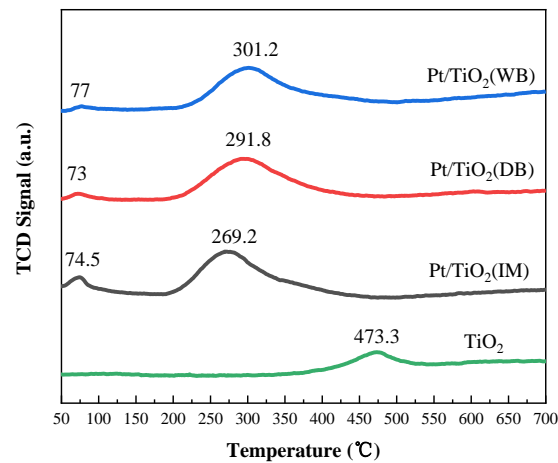


Figure 6. H₂-TPR profiles of TiO₂ and Pt/TiO₂ catalysts.

2.2.6. XPS

The XPS spectra of the Pt 4*f* core level region in the Pt/TiO₂ catalysts prepared by different methods are shown in Figure 7. After peak fitting, doublet peaks were observed in all three spectra, which can be attributed to the PtO peaks at 72.2 and 75.4 eV [39]. This was consistent with the report that the catalysts prepared by anatase TiO₂ have a high content of Pt²⁺ phase on their surfaces [28]. The results of XPS showed that different preparation methods did not change the status of Pt species in the catalyst. The PtO peak intensity for Pt/TiO₂(IM) was higher than that of the other catalysts. It can be speculated that Pt had better dispersion in the catalysts prepared by impregnation. This conclusion is consistent with the TEM images in Figure 5 showing the dispersion of Pt on all three catalysts. It can also be inferred that the surface Pt content of the Pt/TiO₂(IM) catalyst was higher than that of the other two Pt/TiO₂ catalysts, as well as that Pt/TiO₂(IM) had a higher utilization rate of Pt. This is supported by the catalyst results for CO oxidation shown in Figure 1.

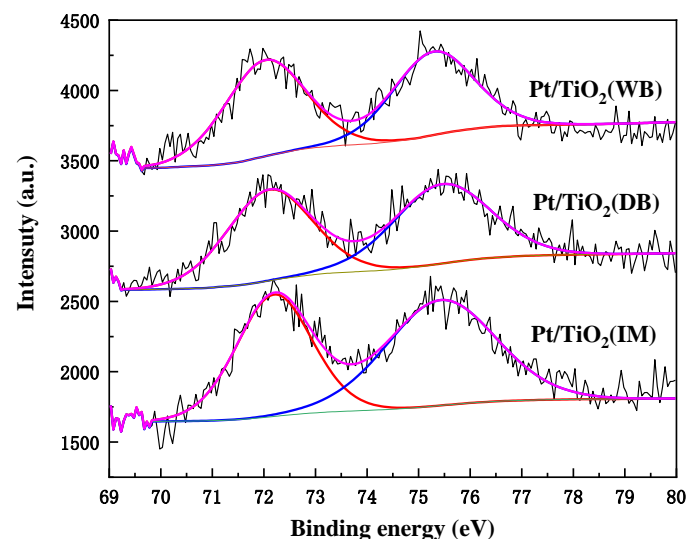


Figure 7. XPS profiles of core level spectra of Pt 4*f* for Pt/TiO₂ catalysts.

The XPS spectra of the S2*p* core level region in the Pt/TiO₂(IM) and Pt/TiO₂(IM)-SH catalysts are shown in Figure 8. SO₄²⁻ and SO₃²⁻ peaks appear for both the fresh and poisoned catalysts. The SO_x²⁻ peaks in the spectrum of Pt/TiO₂(IM) originated from impurities in the TiO₂ carrier. The intensity of these peaks in the spectrum of Pt/TiO₂(IM)-SH significantly increased compared with the fresh catalyst spectrum, an indication of a much higher surface concentration of SO₄²⁻ and SO₃²⁻. This further verified the poisoning

mechanism for Pt/TiO₂ catalysts in the presence of SO₂. The catalyst was poisoned but not deactivated. The reason may be as follows: SO₂ could inhibit the catalytic oxidation of CO, but H₂O could enhance the catalytic oxidation of CO. The promoting effect of H₂O was greater than the inhibiting effect of SO₂ in the presence of SO₂ and water vapor, so as the test progressed, the amount of sulfate on Pt/TiO₂ did not continue to increase.

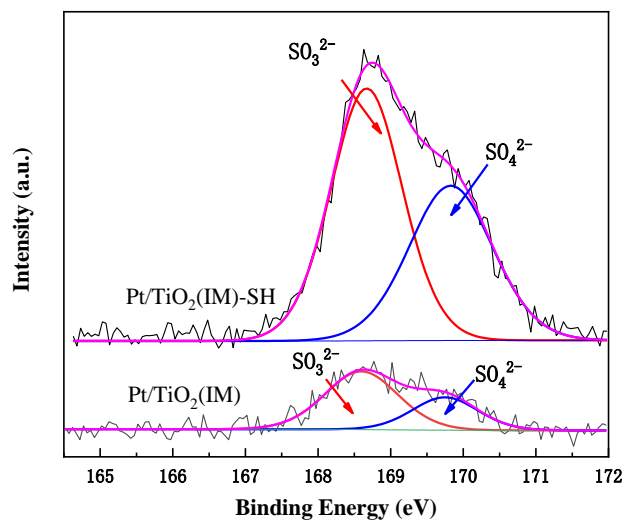


Figure 8. XPS profiles of core level spectra of S2p for Pt/TiO₂(IM) and Pt/TiO₂(IM)-SH.

2.2.7. SO₂-TPD

In order to investigate the adsorption performance of the catalysts for SO₂, SO₂-TPD tests were carried out on all three catalysts, as shown in Figure 9. The three catalysts showed SO₂ desorption peaks between 50 and 450 °C. The peak between 50 and 200 °C represents the desorption of physically adsorbed SO₂ and the peak between 200 and 450 °C represents the desorption of moderate sulfate [40,41]. Integrating the curves, the order of the SO₂ desorption peak area of the three catalysts is as follows: Pt/TiO₂(WB) > Pt/TiO₂(DB) > Pt/TiO₂(IM). Therefore, the order of adsorption strength of the three catalysts for SO₂ follows the same trend. It is worth noting that Pt/TiO₂(WB) was found to have a stronger adsorption capacity of SO₂ than Pt/TiO₂(DB) but a slower decay rate in CO oxidation catalytic efficiency in the presence of SO₂ and water. While the preparation method had an effect on the adsorption capacity of SO₂, the decay rate of CO oxidation catalytic efficiency in the presence of SO₂ and H₂O was dependent on not only the adsorption capacity of SO₂ but also the interaction of the physical structure and chemical properties of the catalysts. Nevertheless, these results show that the most stable catalyst for oxidation of CO in the presence of SO₂ and H₂O, Pt/TiO₂(IM), also demonstrated the lowest adsorption strength for SO₂.

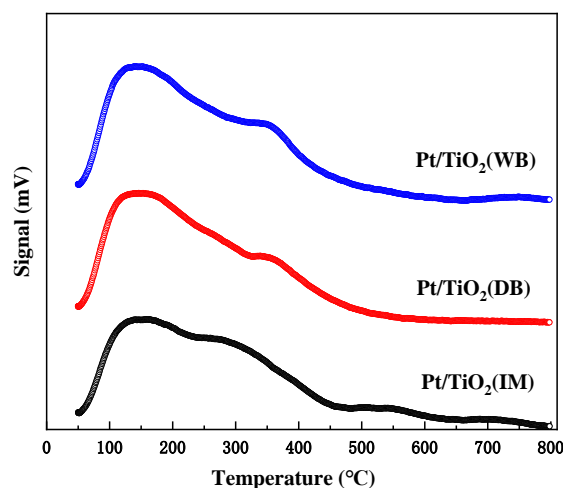


Figure 9. SO_2 -TPD profiles of $\text{Pt}/\text{TiO}_2(\text{IM})$, $\text{Pt}/\text{TiO}_2(\text{DB})$ and $\text{Pt}/\text{TiO}_2(\text{WB})$ catalysts.

3. Materials and Methods

3.1. Catalyst Preparation

A series of Pt/TiO_2 catalysts with a theoretical Pt content of 0.9 wt.% were prepared by impregnation ($\text{Pt}/\text{TiO}_2(\text{IM})$), dry ball mill ($\text{Pt}/\text{TiO}_2(\text{DB})$), and wet ball mill ($\text{Pt}/\text{TiO}_2(\text{WB})$).

$\text{Pt}/\text{TiO}_2(\text{IM})$ catalysts were prepared as follows: The commercial TiO_2 (Chongqing Beiteng Industry and Trade Co., Ltd. China) was added to a H_2PtCl_6 (China National Pharmaceutical Group Corporation, Beijing, China) aqueous solution, and the resulting suspension was ultrasonic stirred for 3 h in a water bath at 70 °C. After impregnation, the suspension was dried at 110 °C with a blow drying oven and then treated at 450 °C for 2 h to obtain the $\text{Pt}/\text{TiO}_2(\text{IM})$ catalyst.

$\text{Pt}/\text{TiO}_2(\text{DB})$ catalysts were prepared as follows: a mixture of H_2PtCl_6 and the commercial TiO_2 were added to a ball mill pot and ball milled at 500 r/min for 1 h. After ball milling, the resulting powder was treated at 450 °C for 2 h to obtain the $\text{Pt}/\text{TiO}_2(\text{DB})$ catalyst.

$\text{Pt}/\text{TiO}_2(\text{WB})$ catalysts were prepared as follows: The commercial TiO_2 was added to a H_2PtCl_6 solution, and the resulting suspension was added to a ball mill pot. Ball milling occurred at 500 r/min for 1 h. After ball milling, the suspension was dried at 110 °C with a blow drying oven and then treated at 450 °C for 2 h to obtain the $\text{Pt}/\text{TiO}_2(\text{WB})$ catalyst.

3.2. Catalyst Characterization

The surface areas of the catalysts were determined by the BET method with a Micromeritics Gemini V instrument (USA). XRD patterns were recorded with a Bruker D8 Advance instrument (Germany) operated at 40 kV and 40 mA using nickel-filtered $\text{Cu K}\alpha$ radiation ($\lambda = 0.15406$ nm). The morphology of the catalysts was observed by a JEM-00F SEM instrument (Japan) operating at 20 kV. The samples were coated with gold for 30 s before measurement. TEM was also used to observe catalyst morphology (JEM 2100F, Japan). CO chemisorption tests were used to determine the dispersion and particle size of platinum, using an AutoChem II 2920 chemisorption instrument (USA). The chemisorption experimental method was as follows: 100 mg of sample (40–60 mesh) were reduced in a 10% H_2 atmosphere for 1 h, cooled to 50 °C, and purged with argon for 15 min, followed by a pulse adsorption test using a 10% CO -He mixture. Temperature programmed reduction (H_2 -TPR) was performed with the same AutoChem II 2920 instrument (USA). The H_2 -TPR experimental steps were as follows: 50 mg of sample (40–60 mesh) were pretreated at 200 °C in air for 30 min, cooled to room temperature, and purged with He for 15 min. After pretreatment, the H_2 -TPR test was performed with a 10% H_2 -He mixture and a 10 °C/min heating rate using a thermal conductivity detector to measure hydrogen consumption. The surface chemical states of the Pt/TiO_2 catalysts were investigated by XPS (ESCALAB 250Xi, United Kingdom) using an Al $\text{K}\alpha$ X-ray source (1486.7 eV) at 15 kV and 25 W with the binding energy calibrated by C1s at 284.8 eV. The SO_2 adsorption capacity of the

catalysts was investigated by temperature programmed desorption (SO₂-TPD) using an Autosorb-iQ-C chemisorption analyzer (Quantachrome, USA). The SO₂-TPD experimental steps were as follows: 50 mg of sample (40–60 mesh) were pretreated at 300 °C in an He atmosphere for 60 min and cooled to 50 °C. A 2% SO₂-He gas mixture was passed over the catalyst sample for 1 h to ensure SO₂ saturation and then purged with He purge for 1 h to remove physically adsorbed SO₂. The sample was then heated from 50 to 800 °C under He for testing.

3.3. Evaluation of Catalytic Performance

CO oxidation was carried out in a continuous flow fixed-bed quartz reactor. The mass of the catalyst was 1.8760 g. The total gas flow rate was 1500 cm³/min, and the simulated flue gas was 10,000 mg/m³ CO and 15.6% O₂ in N₂. An MRU infrared flue gas analyzer (MGA6 Plus, Germany) was used to monitor the CO concentration at the outlet. The CO removal efficiency was calculated by the following equation:

$$\eta = \frac{C_{in} \times Q_{in} - C_{out} \times Q_{out}}{C_{in} \times Q_{in}} \times 100\% \quad (1)$$

where C_{in} is the inlet CO concentration of the catalyst, Q_{in} is the inlet flue gas volume of the catalyst, C_{out} is the outlet CO concentration of the catalyst, and Q_{out} is the outlet flue gas volume of the catalyst.

The sulfur and water resistance of the catalyst were evaluated by adding 15% water vapor and 50 ppm of SO₂ to the simulated flue gas at 170 °C.

4. Conclusions

This study shows that the preparation method of supported Pt/TiO₂ catalysts has a significant effect on the catalytic performance for the oxidation of CO. Loading Pt on TiO₂ by impregnation (Pt/TiO₂(IM)) resulted in the smallest impact on the pore structure of TiO₂ compared with dry ball milling and wet ball milling methods. Pt/TiO₂(IM) also had the highest BET surface area, largest pore volume, largest pore size, highest level of Pt dispersion, and smallest Pt particle size compared with Pt/TiO₂ produced by other methods. In addition, Pt/TiO₂(IM) demonstrated the lowest SO₂ adsorption capacity. As a catalyst, Pt/TiO₂(IM) showed the best catalytic performance for the oxidation of CO at low temperatures and the highest stability in the presence of SO₂ and water vapor. In future research, the preparation method of the catalyst should be further optimized, and other modification treatment methods, such as the introduction of additives and catalyst pretreatment, should be combined to improve the performance and life of the catalyst, which is the key to promote the application of the Pt/TiO₂ catalyst in flue gas containing SO₂.

Author Contributions: Conceptualization, J.C. and J.L.; methodology, J.C. and J.L.; software, J.C. and Z.Y.; validation, J.C. and J.L.; formal analysis, J.C. and Z.Y.; investigation, J.C., Z.Y. and J.L.; resources, J.L.; data curation, J.C., Z.Y. and J.L.; writing—original draft preparation, J.C. and Z.Y.; writing—review and editing, J.L.; supervision, J.L.; project administration, J.L.; funding acquisition, J.L. All authors have read and agreed to the published version of the manuscript.

Funding: This research was funded by Sinosteel Tiancheng Environmental Protection Science & Technology Co. Ltd.

Conflicts of Interest: The authors declare no conflict of interest.

References

1. Lee, H.U.; Choi, J.H.; Yeo, Y.K.; Song, H.G.; Na, B.G. Effect of Evacuation and Rinse Conditions on Performance in PSA Process for CO₂ Recovery. *Korean Chem. Eng. Res.* **2000**, *38*, 809–816.
2. Oommen, L.P.; Narayanappa, K.G. Assimilative Capacity approach for air pollution control in automotive engines through magnetic field-assisted combustion of hydrocarbons. *Environ. Sci. Pollut. Res.* **2021**. [[CrossRef](#)]

3. Dey, S.; Chandra, D.G. Controlling carbon monoxide emissions from automobile vehicle exhaust using copper oxide catalysts in a catalytic converter. *Mater. Today Chem.* **2020**, *17*. [[CrossRef](#)]
4. Nguyen, V.; Salama, M.; Fernandez, D.; Sperling, J.D.; Regina, A.; Rivera, R.; Wang, J.; Friedman, B.W.; Smith, S.W. Comparison between carbon monoxide poisoning from hookah smoking versus other sources. *Clin. Toxicol.* **2020**, *58*, 1320–1325. [[CrossRef](#)] [[PubMed](#)]
5. Yang, C.; Zhao, Z.Z.; Liu, Q.J. Theoretical study of CO oxidation on Au-1/Co₃O₄ (110) single atom catalyst using density functional theory calculations. *Mater. Sci. Semicond. Process.* **2020**, *123*. [[CrossRef](#)]
6. Gao, F.Y.; Yan, H.; Tang, X.L.; Yi, H.H.; Zhao, S.Z.; Yu, Q.J.; Ni, S.Q. Simultaneous removal of gaseous CO and elemental mercury over Cu-Co modified activated coke at low temperature. *J. Environ. Sci.* **2021**, *101*, 36–48. [[CrossRef](#)] [[PubMed](#)]
7. Li, J.; Ma, Z.F.; Liu, X.Q.; Yao, H.Q. Density functional theory calculations of carbon monoxide adsorption on activated carbon loaded with cuprous salt. *Acta Chim. Sin.* **2005**, *63*, 903–908.
8. Huang, S. Optimization and improvement of carbon monoxide cryogenic separation process. *Mod. Chem. Ind.* **2019**, *39*, 185–188.
9. Hogendoorn, J.A.; Swaaij, W.P.M.V.; Versteeg, G.F. The absorption of carbon monoxide in COSORB solutions: Absorption rate and capacity. *Chem. Eng. J. Biochem. Eng. J.* **1995**, *59*, 243–252. [[CrossRef](#)]
10. Khan, F.I.; Ghoshal, A.K. Volatile organic compounds control: Best possible techniques. *Chem. Eng. World* **1999**, *34*, 103–124.
11. Saavedra, J.; Whittaker, T.; Chen, Z.F.; Pursell, C.J.; Rioux, R.M.; Chandler, B.D. Controlling activity and selectivity using water in the Au-catalysed preferential oxidation of CO in H₂. *Nat. Chem.* **2016**, *8*, 584–589. [[CrossRef](#)]
12. Guan, H.L.; Lin, J.; Li, L.; Wang, X.D.; Zhang, T. Highly active subnano Rh/Fe(OH)_x catalyst for preferential oxidation of CO in H₂-rich stream. *Appl. Catal. B Environ.* **2016**, *184*, 299–308. [[CrossRef](#)]
13. Wang, C.; Gu, X.K.; Yan, H.; Yue, L.; Liu, J. Water-mediated Mars-Van Krevelen mechanism for CO oxidation on Ceria supported single-atom Pt1 Catalyst. *Acs Catal.* **2017**, *7*, 887–891. [[CrossRef](#)]
14. Lou, Y.; Liu, J.Y. A highly active Pt-Fe/γ-Al₂O₃ catalyst for preferential oxidation of CO in excess of H₂ with a wide operation temperature window. *Chem. Commun.* **2017**, *53*, 9020–9023. [[CrossRef](#)] [[PubMed](#)]
15. Chen, Y.; Lin, J.; Pan, X.; Zhang, T. Local structure of Pt species dictates remarkable performance on Pt/Al₂O₃ for preferential oxidation of CO in H₂. *Appl. Catal. B Environ.* **2021**, *282*. [[CrossRef](#)]
16. Kim, H.J.; Jang, M.G.; Shin, D.; Han, J.W. Design of Ceria Catalysts for Low-Temperature CO Oxidation. *ChemCatChem* **2020**, *12*, 11–26. [[CrossRef](#)]
17. Ince, T.; Uysal, G.; Akin, A.N.; Ldirim, R.Y. Selective low temperature CO oxidation over Pt-Co-Ce/Al₂O₃ in hydrogen rich stream. *Appl. Catal. Gen.* **2005**, *292*, 171–176. [[CrossRef](#)]
18. Son, I.H.; Lane, A.M.; Johnson, D.T. The study of the deactivation of water-pretreated Pt/g-Al₂O₃ for low-temperature selective CO oxidation in hydrogen. *J. Power Sources* **2003**, *124*, 415–419. [[CrossRef](#)]
19. Boubnov, A.; Dahl, S.; Johnson, E.; Molina, A.P.; Simonsen, S.B.; Cano, A.; Helveg, F.M.; Lemus-Yegres, L.J.; Grunwaldt, J. Structure activity relationships of Pt/Al₂O₃ catalysts for CO and NO oxidation at diesel exhaust conditions. *Appl. Catal. B Environ.* **2012**, *126*, 315–325. [[CrossRef](#)]
20. Liu, H.; Zhou, Y.; Zhang, Y.; Bai, L.; Tang, M. Effect of Preparation Processes on Catalytic Performance of PtSnNa/ZSM-5 for Propane Dehydrogenation. *Ind. Eng. Chem. Res.* **2009**, *48*, 5598–5603. [[CrossRef](#)]
21. Abdelsayed, V.; Saoud, K.M.; El-Shall, M.S. Vapor phase synthesis and characterization of bimetallic alloy and supported nanoparticle catalysts. *J. Nanopart. Res.* **2006**, *8*, 519–531. [[CrossRef](#)]
22. Min, B.K.; Friend, C.M. Heterogeneous Gold-Based Catalysis for Green Chemistry: Low Temperature CO Oxidation and Propene Oxidation. *Chem. Rev.* **2007**, *107*, 2709–2724. [[CrossRef](#)]
23. Dey, S.; Dhal, G.C. Property and structure of various platinum catalysts for low-temperature carbon monoxide oxidations. *Mater. Today Chem.* **2020**, *16*. [[CrossRef](#)]
24. Hong, X.W.; Sun, Y. Effect of Preparation Methods on the Performance of Pt/CeO₂ Catalysts for the Catalytic Oxidation of Carbon Monoxide. *Catal. Lett.* **2016**, *146*, 2001–2008. [[CrossRef](#)]
25. Smirnov, M.Y.; Kalinkin, A.V.; Pashis, A.V.; Prosvirin, I.P.; Bukhtiyarov, V.I. Interaction of SO₂ with Pt Model Supported Catalysts Studied by XPS. *J. Phys. Chem. C.* **2014**, *118*, 22120–22135. [[CrossRef](#)]
26. Taira, K.; Einaga, H. The Effect of SO₂ and H₂O on the Interaction Between Pt and TiO₂(P-25) During Catalytic CO Oxidation. *Catal. Lett.* **2019**, *149*, 965–973. [[CrossRef](#)]
27. Qi, L.F.; Cheng, B.; Yu, J.G.; Ho, W.K. High-surface area mesoporous Pt/TiO₂ hollow chains for efficient formaldehyde decomposition at ambient temperature. *J. Hazard. Mater.* **2016**, *301*, 522–530. [[CrossRef](#)] [[PubMed](#)]
28. Su, Y.; Ji, K.M.; Xun, J.Y.; Zhang, K.; Li, P.; Zhao, L. Catalytic oxidation of low concentration formaldehyde over Pt/TiO₂ catalyst. *Chin. J. Chem. Eng.* **2021**, *29*, 190–195. [[CrossRef](#)]
29. Qi, L.F.; Yu, J.G.; Mietek, J. Preparation and enhanced visible-light photocatalytic H₂-production activity of CdS-sensitized Pt/TiO₂ nanosheets with exposed (001) facets. *Phys. Chem. Chem. Phys.* **2011**, *13*, 8915–8923. [[CrossRef](#)] [[PubMed](#)]
30. Qiao, B.; Wang, A.; Yang, X.; Allard, L.F.; Jiang, Z.; Cui, Y.; Liu, J.; Li, J.; Tao, Z. Single-atom catalysis of CO oxidation using Pt1/FeOx. *Nat. Chem.* **2011**, *3*, 634–641. [[CrossRef](#)] [[PubMed](#)]
31. Wang, Z.W.; Bi, L.I.; Chen, M.S.; Weng, W.Z.; Wan, H.L. Size and support effects for CO oxidation on supported Pd catalysts. *Sci. China Chem.* **2010**, *53*, 2047–2056. [[CrossRef](#)]

32. Corma, A.; Concepción, P.; Boronat, M.; Sabater, M.J.; Navas, J.; Yacaman, M.J.; Larios, E.; Posadas, A.; López-Quintela, M.A.; Buceta, D.; et al. Exceptional oxidation activity with size-controlled supported gold clusters of low atomicity. *Nat. Chem.* **2013**, *5*, 775–781. [[CrossRef](#)]
33. Cargnello, M.; Doan-Nguyen, V.V.T.; Gordon, T.R.; Diaz, R.E.; Stach, E.A.; Gorte, R.J.; Fornasiero, P.; Murray, C.B. Control of metal nanocrystal size reveals metal-support interface role for ceria catalysts. *Science* **2013**, *341*, 771–773. [[CrossRef](#)]
34. Zhang, C.; He, H.; Tanaka, K.I. Catalytic performance and mechanism of a Pt/TiO₂ catalyst for the oxidation of formaldehyde at room temperature. *Appl. Catal. B Environ.* **2006**, *65*, 37–43. [[CrossRef](#)]
35. Epling, W.S.; Cheekatamarla, P.K.; Lane, A.M. Reaction and surface characterization studies of titania-supported Co, Pt and Co/Pt catalysts for the selective oxidation of CO in H₂-containing streams. *Chem. Eng. J.* **2003**, *93*, 61–68. [[CrossRef](#)]
36. Zhu, X.; Shen, M.; Lobban, L.L.; Mallinson, R.G. Structural effects of Na promotion for high water gas shift activity on Pt-Na/TiO₂. *J. Catal.* **2011**, *278*, 123–132. [[CrossRef](#)]
37. Wang, L.; Sakurai, M.; Kameyama, H. Study of catalytic decomposition of formaldehyde on Pt/TiO₂ alumite catalyst at ambient temperature. *J. Hazard. Mater.* **2009**, *167*, 399–405. [[CrossRef](#)] [[PubMed](#)]
38. Alonso, F.; Riente, P.; Rodríguez-Reinoso, F.; Ruiz-Martínez, J.; Sepúlveda-Escribano, A.; Yus, M. Platinum nanoparticles supported on titania as an efficient hydrogen-transfer catalyst. *J. Catal.* **2008**, *260*, 113–118. [[CrossRef](#)]
39. Pels, J.R.; Kapteijin, F.; Moulijn, J.A.; Zhu, Q.; Thomas, K.M. Evolution of nitrogen functionalities in carbonaceous materials during pyrolysis. *Carbon* **1995**, *33*, 1641–1653. [[CrossRef](#)]
40. Peng, Y.; Wang, D.; Li, B.; Wang, C.; Li, J.; Crittenden, J.C.; Hao, J. Impacts of Pb and SO₂ poisoning on CeO₂-WO₃/TiO₂-SiO₂ SCR catalyst. *Environ. Sci. Technol.* **2017**, *51*, 11943. [[CrossRef](#)]
41. Chen, L.Q.; Li, R.; Li, Z.B.; Yuan, F.L.; Niu, X.Y.; Zhu, Y.J. Effect of Ni doping in Ni_xMn_{1-x}Ti₁₀ (x= 0.1-0.5) on activity and SO₂ resistance for NH₃-SCR of NO studied with in situ DRIFTS. *Catal. Sci. Technol.* **2017**, *7*, 3243–3257. [[CrossRef](#)]